Modulating the Reduction Potential and Ligand Basicity of Ni(II) HER Catalysts with Highly Conjugated N_2S_2 Ligands

Mohan Paudel,[a] Sanjit Karki,[a] Kritika Bajaj,[a] Dillon T. Hofsommer,[a] Saurav Parmar,[a] Mark S. Mashuta,[a] Pawel M. Kozlowski,[a] Gautam Gupta,[b] Robert M. Buchanan,[a] Craig A. Grapperhaus[a]**

[a]Department of Chemistry, University of Louisville, 2320 S. Brook St, Louisville, KY 40292.

[b]Department of Chemical Engineering, University of Louisville, Louisville, Kentucky 40292.

KEYWORDS: redox non innocent ligands, N_2S_2 chelate ligands, reduction potential modulation, hydrogen evolution reaction, density functional theory

Abstract

Molecular catalysts with N_2S_2 chelates and earth abundant metals have been used in different applications. With their versatile nature to modulate the activity through the changes in ligand framework, they are excellent candidates to generate low-cost and sustainable energy as electrocatalysts for the hydrogen evolution reaction (HER). Herein we demonstrate the modulation of the reduction potential and basicity across a series of six square planar Ni(II) complexes with bis(thiosemicarbazonato) (BTSC), hybrid thiosemicarbazonato-alkylthiocarbamato (TSTC), and bis(alkylthiocarbamato) (BATC) ligands and evaluate their activity as homogenous HER catalysts. The redox active ligands have been designed to modulate the electronic structure of the N_2S_2Ni core and to systematically alter their respective pK_a values. Cyclic voltammograms of all six complexes show two reversible reduction events in acetonitrile that systematically shift to more anodic potentials when the pendent methylthiosemicarbazonato (-NNHC(S)NHMe) groups are substituted with ethylthiocarbamato (-NNHC(S)OEt) groups and/or when the 2,4-butanedione backbone is replaced by 1-phenyl-1,2-propandione. Ligand basicity was evaluated by spectroscopic titration in acetonitrile and found to vary systematically across the series. Within the series of complexes the reduction potentials vary over an ~500 mV range and the ligand basicity over ~7 pK_a units. Density functional theory (DFT) computations are consistent with experimental changes in redox potential and pK_a values across the series of complexes. The results demonstrate a unique example in which electronic properties of the complexes are modulated via small ligand structure variations. The complexes are stable under acidic conditions or upon reduction, but they degrade upon reduction in the presence of acid limiting their application as homogeneous HER electrocatalysts.

Introduction

Molecular catalysts containing N_2S_2 chelates coordinated with earth abundant metals have been the subject of many studies involving electron transfer processes.[1] In particular, bis(thiosemicarbazonato) (BTSC) complexes have attracted much recent attention due to their redox non-innocent behavior.[2,3] They are a class of N_2S_2 ligands obtained from the condensation of two thiosemicarbazide molecules with a α-dicarbonyl backbone that can bind an array of metals to generate BTSC metal complexes with rigidly square planar geometries as observed for Ni(II) (Figure 1).[4] The modular nature of their structures with multiple sites for variation has led to their use in different medicinal and diagnostic applications, such as: treatment of neurodegenerative diseases,[5] hypoxia imaging,[6] and a wide range of pharmacological properties including antitumor,[7] antiviral,[8] antibacterial,[9] and antifungal agents.[10] The ligand backbone (R1 and R2) and the pendent amine groups (R3, and R4) (Figure 1) can be modified to selectively tune the electronic properties of the coordinated metal ion. Bis(alkylthiocarbamato) (BATC) complexes (Figure 1) on the other hand are a more recent group of complexes with N_2S_2 chelates first reported in 2017 by us and are easily prepared by the condensation of a dione backbone with two equivalents of hydrazinecarbothioic acid O-ethyl ester.[11] It is interesting that replacing each pendent amines in BTSCs with alkoxy groups results in an anodic shift of the metal reduction potential (e.g. Cu^{II}/Cu^{I}) by nearly 150 mV per alkoxy unit. Like the BTSC complexes, the Ni(BATC) complexes are also rigidly square planar due to the high degree of ligand π delocalization. In 2020, we also reported the synthesis and properties of a novel group of thiosemicarbazonato/alkylthiocarbamato chelates (TSTC) that possess tunable metal reduction potentials (e.g. Cu^{II}/Cu^{I}) intermittent between their related BTSC/BATC complexes (Figure 1).[12] Overall, this series of compounds share a common N_2S_2 set of donor atoms, have rigidly square planar coordination geometries for their Ni(II)

complexes and relative reduction potentials that span a range of about a 400 mV making them ideal for evaluating the effect of changing backbone and pendent substituents on ligand basicity and electrocatalytic activity for H_2 production.

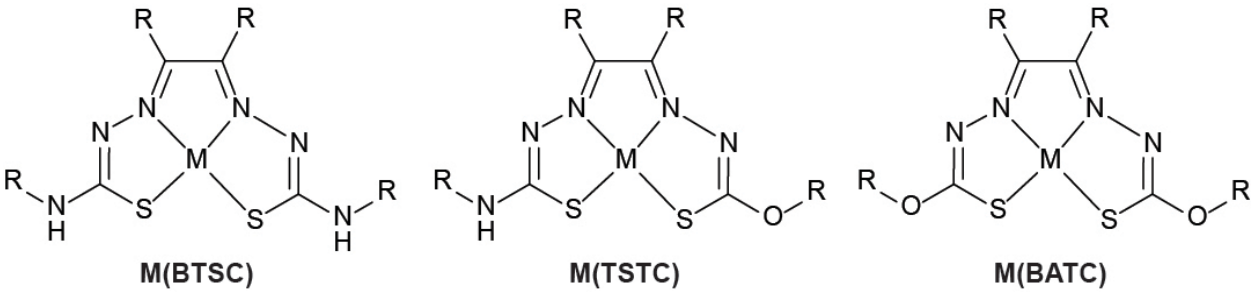

Figure 1. General structure of bis(thiosemicarbazonato) M(BTSC), thiosemicarbazonato/alkylthiocarbamato M(TSTC) and bis(alkylthiocarbamateo) M(BATC) metal complexes.

Recently, our group[13-18] and others[19-22] have reported the electrocatalytic activity of BTSC metal complexes for the hydrogen evolution reaction (HER). The redox activity of the ligand supports a variety of mechanistic pathways including: 1) ligand-assisted metal-centered, where the ligand is an electron reservoir supporting a metal hydride intermediate;[15] 2) metal-assisted ligand-centered, where the metal acts as an electron reservoir for bond making/breaking reactions at the ligand;[14] and 3) ligand-centered, where the ligand alone is responsible for activity with the metal absent or in a structural role.[13] Previously, we reported a ligand-assisted metal-centered mechanism for the Ni(BTSC) complex **1**.[15] Interestingly, Orio and coworkers observed a ligand-centered mechanism for a series of Ni(BSTC) complexes in which the -NHMe substituent of **1** is replaced with -NHPh^R groups (Ph^R = *p*-$C_6H_5OCH_3$, *p*-$C_6H_5SCH_3$, *p*-C_6H_5CN).[19] We also observed ligand-centered HER for the related complex Ni(DMTH) (DMTH = diacetyl-2-(4-methyl-3-thiosemicarbazonato)-3-(2-pyridinehydrazonato), in which one of the thiosemicarbazonato donors in **1** is substituted with a 2-pyridinehydrazonato donor.[23]

Therefore, it is of interest to see if changes in ligand electronic structure and basicity across the series of structurally related BTSC, TSTC and BATC Ni(II) complexes will influence the pathway for H_2 production during catalysis. The catalytic activity of redox active M(TSTC) and M(BATC) complexes have not been previously evaluated and are part of the study described herein. In this work, we report a series of Ni(II) complexes, **1** – **6** (Figure 2), and evaluate the influence of ligand substitution on their reduction potential and ligand basicity. The ligands have been designed to modulate the electronic structure of the N_2S_2Ni core by variation of the pendent functional groups yielding BTSC, hybrid thiosemicarbazonato-alkylthiocarbamato (TSTC), and bis(alkylthiocarbamato) (BATC) complexes. Further tuning of the electronic structure was accomplished by substitution of the 2,3-butanedione backbone in **1** – **3** with a 1-phenyl-1,2-propandione backbone in **4** – **6**.

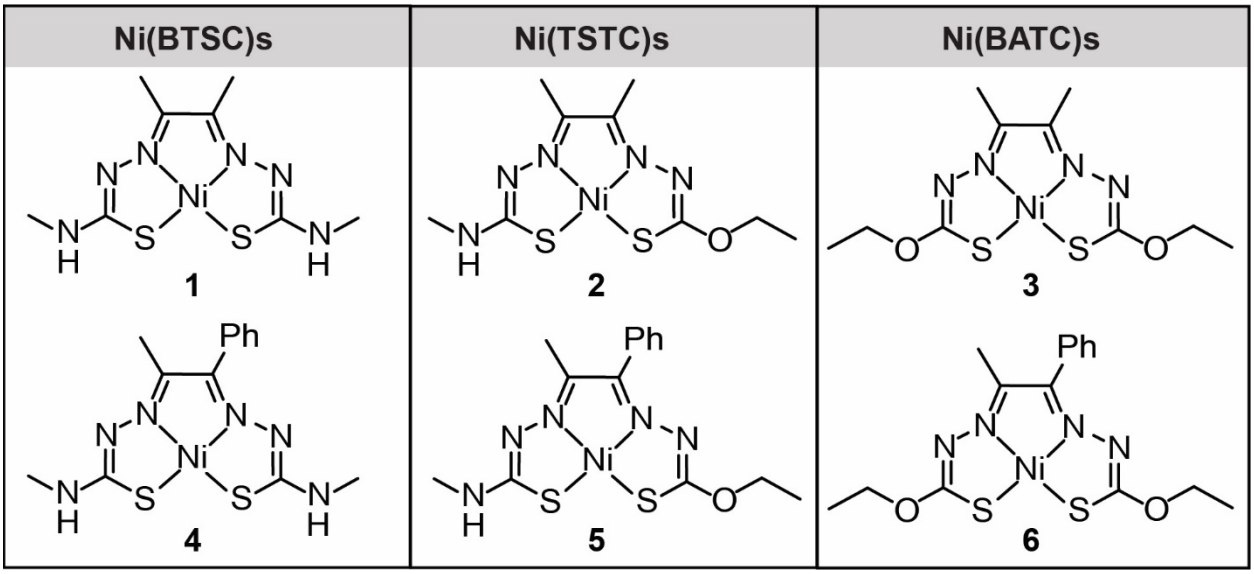

Figure 2. Structures for complexes **1** – **6** in this study.

Experimental

Materials and Methods

All solvents and reagents were purchased from commercial sources and were used as received unless otherwise noted. Solvents were dried using an MBraun solvent purification system. The H_2L^3 ligand,[11] hydrazinecarbothioic acid O-ethyl ester,[24] and complexes **1**,[4] **2**,[12] **4**,[25] and **5**[12] were synthesized according to reported literature procedures. All complexes in this study are air and water stable as solids and did not require protection from the atmosphere.

Synthetic Procedures

1-Phenyl-1,2-propanedione-bis(ethylthiocarbamate) (H_2L^6). 1-Phenyl-1,2-propanedione (2.20 g, 14.8 mmol) and hydrazinecarbothioic acid O-ethyl ester (3.57 g, 29.7 mmol) were suspended in ethanol (30 mL) in a round bottom flask equipped with a stir bar. Concentrated sulfuric acid (4 – 5 drops) was added to the mixture and the solution was stirred overnight to obtain white precipitate. The precipitate was filtered and washed with water followed by ethanol. The solid was dried to obtain the H_2L^6 (2.62 g, 7.43 mmol, 50% yield).^{1}H NMR (DMSO-d_6, 500 MHz) δ (ppm): 1.33 (6H), 2.00 (3H), 4.59 (4H), 7.45 (5H), 11.53 (1H), 12.72 (1H). ^{13}C NMR (DMSO-d_6, 176 MHz, 298 K) δ (ppm): 12.18, 14.03, 18.16, 66.15, 67.40, 127.92, 128.60, 129.30, 135.92, 146.42, 147.79, 186.65, 189.67. FT-IR (cm^{-1}): 3327 (s, N-H), 3249 (br, N-H), 2984 (s), 2937 (s, C-H) and 1482 (s, C=N), 1403 (m, C=N), 1314 (s, C-N), 1195 (s, C-O), 1071 (m, C=S), 702 (s, C=C). HRMS (m/z) for $[C_{15}H_{20}N_4O_2S_2+Na]^+$: calc.: 375.0926; obs.: 375.0923.

*2,3-Butanedione-bis(ethylthiocarbamato-$\kappa^4(N^1S),(N^2S)$)nickel(II) (**3**)*. In a round bottom flask equipped with a magnetic stir bar was added 100 mg (0.34 mmol) of H_2L^3 in 10 mL methanol. To this was added 85 mg (0.34 mmol) of nickel acetylacetonate tetrahydrate and the mixture was refluxed for 4 hours. After cooling to room temperature, the mixture was filtered to obtain **3** as a red colored solid (97 mg, 0.28 mmol, 81% yield). Single crystals suitable for X-ray crystallography

were grown by slow evaporation method using acetonitrile as solvent. ^{1}H NMR (DMSO-*d*$_6$, 700 MHz, 298 K) δ (ppm): 1.22 (t, 6H, 7 Hz), 1.97 (s, 6H) and 4.24 (q, 4H, 7 Hz). ^{13}C NMR (DMSO-*d*$_6$, 176 MHz, 298 K) δ (ppm): 14.30, 14.66, 69.80, 164.97, 187.90. FT-IR (cm^{-1}): 3675 (br), 2900 (m), 2982 (m, C-H) and 1435 (s), 1314 (m, C=N), 1208 (s,), 1079 (s, C-O), 1012 (s, C-S), 868 (s, Ni-S), 790 (s, Ni-N). UV−vis spectrum in acetonitrile (nm) (M^{-1} cm^{-1}): 252 (40,600), 301 (8,900), 374 (5,900). Anal. Calcd. for $C_{10}H_{16}N_4NiO_2S_2$: C, 34.61; H, 4.65; N, 16.14. Found: C, 34.31; H, 4.91; N, 15.92.

1-Phenyl-1,2-propanedione-bis(ethylthiocarbamato- $\kappa^4(N^1S),(N^2S)$*)nickel(II)* (***6***). In a round bottom flask equipped with reflux condenser was added 100 mg (0.28 mmol) of H_2L^6 in 10 mL ethanol. To this was added 70 mg (0.28 mmol) nickel acetylacetonate tetrahydrate and the mixture was refluxed for 4 hours. After cooling to room temperature, the mixture was filtered to obtain **6** as a green colored solid (94 mg, 0.23 mmol, 82% yield). Single crystals suitable for X-ray crystallography were grown by slow evaporation method using saturated acetonitrile solution. ^{1}H NMR (DMSO-*d*$_6$, 700 MHz, 298 K) δ (ppm): 1.13 (t, 3H, 7 Hz), 1.24 (t, 3H, 7 Hz), 1.84 (s, 3H), 4.04 (q, 2H, 7 Hz), 4.27 (q, 2H, 7 Hz) and 7.49 (m, 5H). ^{13}C NMR (DMSO-*d*$_6$, 176 MHz, 298 K) δ (ppm): 14.27, 14.39, 16.25, 69.92, 69.97, 128.06, 128.95, 129.17, 130.40, 161.75, 164.67, 187.82, 189.50. FT-IR (cm^{-1}): 3675 (br), 2900 (m), 2987 (m, C-H), 1435 (s), 1304 (m, C=N), 1225 (s), 1128 (m, C=O), 1020 (s, C-S), 870 (m, Ni-S), 789 (m, Ni-N). UV−vis spectrum in acetonitrile (nm) (M^{-1} cm^{-1}): 254 (30,600), 301 (8,900), 348 (7,200). Anal. Calcd. for $C_{15}H_{18}N_4NiO_2S_2$: C, 44.03; H, 4.43; N, 13.69. Found: C, 44.02; H, 4.38; N, 14.18.

Physical Methods

The ^{1}H and ^{13}C NMR data were collected on a Varian Inova 500 MHz and 700 MHz NMR spectrometer using deuterated solvents (Cambridge Isotopes). Elemental analyses were performed by Micro-Analysis Inc. (Wilmington, DE) by combusting the sample on a calibrated microbalance based on the methodologies of Pregl (CH) and Dumas (N) (CHN: ASTM D5291). Electronic spectra were collected as solutions in acetonitrile in 1 cm quartz cuvette using Agilent 8453 diode array spectrometer. Infrared spectra were recorded on a Thermo Nicolet Avatar 360 spectrometer with an ATR attachment (4 cm^{-1} resolution). The molar absorptivity (ε) values for **1** – **6** and their protonated derivatives **[1-H]**$^{+}$ – **[6-H]**$^{+}$ were determined from UV-visible spectra collected at different concentrations in acetonitrile. The pK_a values were determined through spectrophotometric titration of the colored compounds with a stock solution of hydrogen triphenylphosphonium tetrafluoroborate (pK_a MeCN = 7.62).[26] (See the Supporting Information for example pK_a calculations)

Electrochemical Measurements

Voltammetry. Cyclic voltammetry (CV) and square wave voltammetry (SWV) data were collected using a Gamry 1000 Interface potentiostat/galvanostat using a three-electrode cell with a glassy carbon working electrode, Ag wire quasi-reference electrode, and a Pt wire counter electrode. The glassy carbon electrode (GCE) was polished with an aqueous alumina slurry, rinsed with water, acetonitrile, and air dried prior to use. The glassy carbon electrode was polished after each scan to remove any adhered substances. All CVs are referenced against the ferrocenium/ferrocene (Fc^{+}/Fc^{0}) standard couple as an internal standard. In a typical electrochemical experiment, 0.3 mM catalyst was dissolved in 25 mL of acetonitrile containing 0.1 M tetrabutylammonium hexafluorophosphate (Bu_4NPF_6) as the supporting electrolyte. The solution was sparged with argon for 15 min to remove dissolved oxygen prior to data collection.

Hydrogen Evolution Reaction. Solutions of the catalyst were prepared for analysis by CV as described in the preceding section. Then, aliquots of glacial acetic acid were added. After each addition, the solution was stirred for 15 s prior to data collection. CVs were recorded at a scan rate of 0.200 V/s. For ease of comparison, all HER activity was evaluated at a consistent acid concentration of 350 m M. The $E_{cat/2}$ value was determined as the potential at which half of the maximum catalytic current is obtained in the presence of 350 mM acetic acid. The catalyst overpotential was determined by subtracting $E_{cat/2}$ by the hydrogen standard reduction potential (calculated as -1.23 V vs Fc^{+}/Fc under these conditions) (See calculation in Supporting Information) following the method by Artero and coworkers[27] compensating for the homoconjugation of acetic acid (pK_a MeCN = 23.5[28]). Maximum turnover frequency (TOF_{max}) was calculated using a method by Dubois et al.[29] and Savéant et al.[30]

Mercury Dip Test. Chronopotentiometry (CA) was carried out at a constant potential of $E_{cat/2}$ for two hours under 350 mM acetic acid and 0.3 mM complex in a three-electrode setup as described above. After the CA experiment, the electrode was rinsed with acetonitrile and used as the working electrode in a blank solution containing 350 mM acetic acid to record the CV. The electrode was then again rinsed with acetonitrile and soaked in metallic mercury for 6 hours. CVs of the mercury treated electrode were recorded in the blank solution containing 350 mM acetic acid in different time intervals (Fig. S25).

Computational Methods

Density functional theory (DFT)[31,32] was used to calculate electronic structures for **1** – **6** and their protonated/reduced derivatives to provide insight into the HER reactions. The accuracy of the DFT is largely dependent on the choice of a proper functional. To determine the proper functional for

the present systems, a series of functionals were used to compare geometric parameters as well as redox potential and pK_a values. Functionals evaluated include: B3LYP,[33-35] B3P86,[36] B3PW91,[37] B97D,[38] BP86,[36] M06,[39] M06-L,[39] and ωB97XD.[40] The 6-311g(d, p)[41,42] and TZVP[43] basis sets were used with each functional for all calculations. A PCM solvation model (acetonitrile) was employed for all the solution phase calculations.[44] Frequency calculations based on optimized geometries contained no imaginary frequencies. The calculations were performed using Gaussian 16 program package.[45] Notepad II, ChemCraft,[46] and Gaussview[47] were used to visualize the output of the calculations. Thermodynamic parameters associated with the complexes were evaluated by calculating pK_a values (pK_a) and reduction potentials ($E_{1/2}$). Hydrogen triphenyl phosphonium ($HPPh_3^+$) and PPh_3 were used as conjugated acid-base pairs for the calculation of pK_a values. Reduction potentials were assessed using the Born-Haber cycle and referenced to ferrocene.[48] (See Supporting Information for sample calculations)

Crystallographic Studies

The CrysAlisPro[49] CCD software package was used to acquire a total of 893 twenty-five second frame ω-scan exposures of data for a 0.50 x 0.10 x 0.06 mm^3 purple prism crystal of **3** at 103 K to a $2\theta_{max}$ = 60.28° using monochromated Mo K_α radiation (0.71073 Å) from a sealed tube. Frame data were processed using CrysAlisPro[49] RED to determine final unit cell parameters: a = 8.1479(4) Å, b = 8.7242(4) Å, c = 20.3485(10) Å, α = 90°, β = 97.592(4)°, γ = 90°, V = 4,631.1(2) $Å^3$, D_{calc} = 1.608 Mg/m^3, Z = 4 to produce raw *hkl* data that were then corrected for absorption (transmission min./max. = 0.793 /1.000; μ = 1.647 mm^{-1}) using SCALE3 ABSPACK included in CrysAlisPro.[50] The structure was solved using Patterson methods in the space group $P2_1/n$ using SHELXS[51] and refined by least squares methods on F^2 using SHELXL.[51] Non-hydrogen atoms were refined with anisotropic atomic displacement parameters. Hydrogen atoms were located by

difference maps and refined isotropically. For all 4,201 reflections (R(int) 0.042) the final anisotropic full matrix least-squares refinement on F^2 for 236 variables converged at R1 = 0.046 and wR2 = 0.113 with a GOF of 1.02.

A purple prism 0.50 x 0.24 x 0.22 mm^3 crystal of **6** was mounted on a glass fiber for collection of X-ray data on an Agilent Technologies/Oxford Diffraction Gemini CCD diffractometer. The CrysAlisPro[49] CCD software package (v 1.171.40.67a) was used to acquire a total of 666 7.5 second frame ω-scan exposures of data at 103 K to a $2\theta_{max}$ = 62.52° using monochromated Mo K_α radiation (0.71073 Å) from a sealed tube. Frame data were processed using CrysAlisPro[49] RED to determine final unit cell parameters: a = 7.1819(5) Å, b = 15.2761(10) Å, c = 15.8472(17) Å, α = 90°, β = 90°, γ = 90°, V = 1738.6(3) $Å^3$, D_{calc} = 1.563 Mg/m^3, Z = 4 to produce raw *hkl* data that were then corrected for absorption (transmission min./max. = 0.786/1.00; μ = 1.371 mm^{-1}) using SCALE3 ABSPACK included in CrysAlisPro.[50] The structure was solved by Direct methods in the orthorhombic space group $Pna2_1$ using SHELXS[51] and refined by least squares methods on F^2 using SHELXL.[51] Non-hydrogen atoms were refined with anisotropic atomic displacement parameters. Hydrogen atoms were located by difference maps and refined isotropically. For all 5,652 unique reflections (R(int) 0.032) the final anisotropic full matrix least-squares refinement on F^2 for 289 variables converged at R1 = 0.025 and wR2 = 0.049 with an absolute structure Flack parameter of -0.013(7) and a GOF of 1.02.

Results and Discussion

Synthesis and Characterization

A series of complexes with a common N_2S_2Ni core (Figure 2) have been prepared with different pendent functional groups and ligand backbone substituents to modulate the physical and electronic structures. Variation of the pendent functional groups yields Ni(BTSCs) **1** and **4**,

Ni(TSTCs) **2** and **5**, and Ni(BATCs) **3** and **6**. Complexes **1** – **3** are based on a 2,3-butanedione backbone, whereas **4** – **6** are based on a 1-phenyl-1,2-propandione backbone. The nickel complexes **1** – **6** were synthesized in high yield by refluxing alcohol solutions of the appropriate ligand with nickel acetylacetonate as reported previously[4,12] and in the experimental section. The identity and purity of previously reported complexes was confirmed by ^{1}H and ^{13}C NMR spectroscopy. For newly prepared complexes **3** and **6**, the spectral data are as expected for diamagnetic, square planar d^8-Ni complexes (Figure S1-S8).

Electronic spectra (Figure S9) of the complexes show two distinct bands near 250 nm (ligand to ligand charge transfer band) and 400 nm (ligand to metal charge transfer band) as observed in previous studies.[17,52] Two shoulders are observed near 300 nm and 350 nm.[12,17] The band at 397 nm for **1** shifts to 392 nm for **2** associated with the substitution of one of the -NHMe groups with -OEt. A further shift to 375 nm is observed for **3**, in which both-NHMe groups are replaced with -OEt groups. A similar shift to higher energy is observed for **4** (413 nm) to **5** (401 nm) to **6** (390 nm) as the pendent functional group is varied.

The ligand basicity of **1** – **6** was evaluated by spectrophotometric titrations with hydrogen triphenylphosphonium tetrafluoroborate (pKa MeCN = 7.62)[26] in acetonitrile (detailed calculations are provided in SI). Complexes **1**, **2**, **4**, and **5** were readily protonated with $HPPh_3BF_4$. Upon protonation, the visible bands near 400 nm shifted to higher energy and there was a decrease in the shoulder near 350 nm (Figures 3 and S10). For the BTSC complexes **1** and **4**, pK_a values of 7.43 ± 0.10 and 8.63 ± 0.05, respectively, were determined indicating a slight decrease in basicity upon substitution of one of the methyl backbone substituents with phenyl. The pK_a values for the TSTC complexes **2** and **5** were measured as 7.00 ± 0.07 and 6.76 ± 0.12, respectively (Table S1). These values are lower than their respective BTSC derivatives by 0.43 and 1.87 indicating that

substitution of one -NHMe with -OEt slightly decreases the basicity of the complex. In contrast, substitution of both -NHMe groups with -OEt in the BATC complexes **3** and **6** substantially decreases basicity and no protonation is observed in acetonitrile with $HPPh_3BF_4$ or even with excess sulfuric acid. As detailed in the computational studies, this is attributed to the greater basicity of the thiosemicarbazonato functional groups, which are present in the BTSC and TSTC complexes, as compared to the ethylthiocarbamato groups.

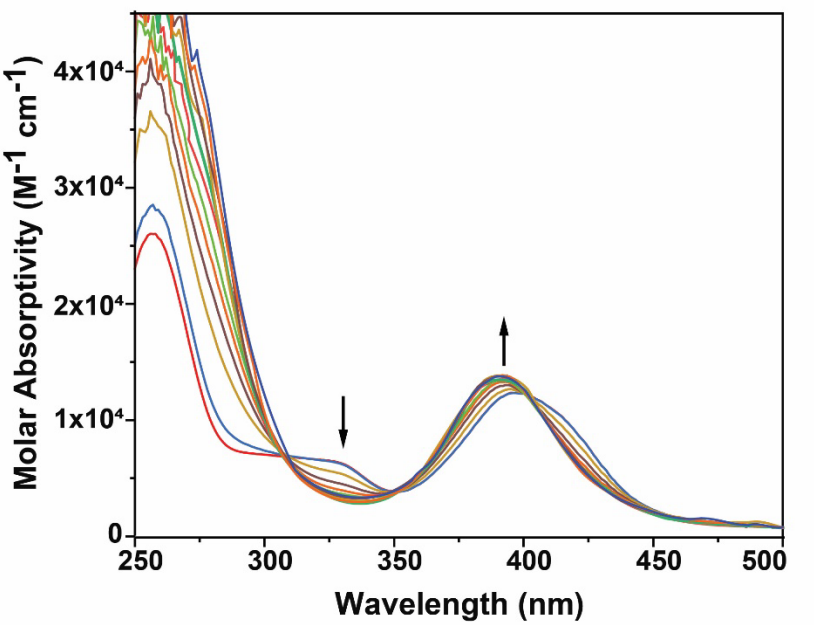

Figure 3. Changes in the electronic spectrum associated with protonation of **1** to **[1-H]**$^+$ during spectrophotometric titration in MeCN with $HPPh_3BF_4$.

Single crystal X-ray diffraction was used to determine the solid-state structure of the new complexes **3** and **6**. Details of the crystallographic studies and structural refinement are provided in the experimental section and Table S2. Figure 4 shows the ORTEP representations of **3** and **6**. For both complexes, the Ni sits in a square planar N_2S_2 coordination environment with alternating single and double bonds within the ligand consistent with extended conjugation. For **3**, the non-

hydrogen atoms are arranged in a rigid square plane with an estimated standard deviation from the least square plane (σ_{plane}) of 0.084 Å. Excluding the phenyl ring, **6** is also best described as planar with a σ_{plane} = 0.042 Å for the non-hydrogen atoms. The phenyl ring of **6** is rotated with respect to the metal-ligand plane with a C1–C2–C4–C5 torsion angle of -130.66(16)º.

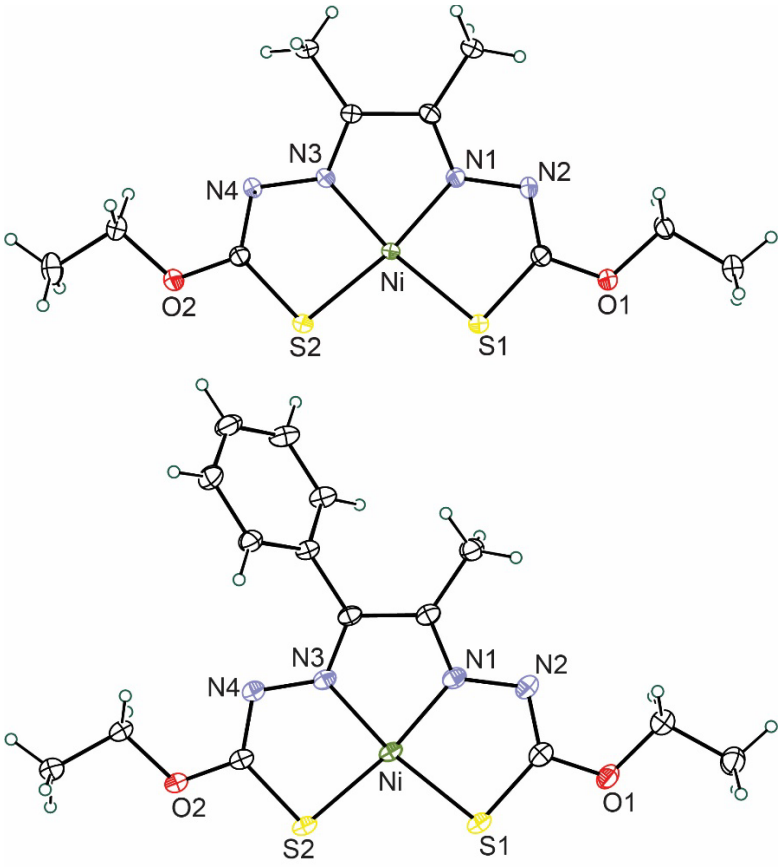

Figure 4. ORTEP view (50% probability) of **3** (top) and **6** (bottom).

A comparison of selected bond distances and angles with the previously reported structures of **1**,[53] **2**,[12] and **5**[12] are provided in Table 1. Across the series, there are only negligible changes in the Ni-N distances, which fall in a narrow range from 1.855(2) – 1.868(3) Å for all complexes. Interestingly, the Ni-S bond distances in the BTSC (**1**) and BATC (**3** and **6**) complexes are statistically equivalent with a small range from 2.1546(6) – 2.1598(7) Å. This indicates that

substitution of the two -NHMe pendent groups with -OEt has virtually no geometric effect. In the hybrid TSTC complexes **2** and **5**, there are slight differences in Ni-S1 and Ni-S2 distances with the bond to the thiosemicarbazonato donor (S1) shorter than the bond to the ethylthiocarbamato donor S2.

Table 1. Selected bond distances (Å) and bond angles (°) for complexes **1** – **6**. Numbers in italics (without esds) represents computational bond length and bond angles for each of the compounds.

	1[53]	**2**[12]	**3**	**4**	**5**[12]	**6**
Bond Lengths (Å)						
Ni1-N1	1.861(2)	1.868(3)	1.861(2)	-	1.851(3)	1.8526(14)
	1.87317	*1.87579*	*1.87360*	*1.86784*	*1.87168*	*1.86966*
Ni1-N3	1.855(2)	1.859(2)	1.857(2)	-	1.863(3)	1.8602(12)
	1.87229	*1.86952*	*1.87341*	*1.87404*	*1.87018*	*1.87418*
Ni1-S1	2.1546(6)	2.1554(8)	2.1575(8)	-	2.1571(9)	2.1535(4)
	2.18834	*2.18868*	*2.19334*	*2.18891*	*2.18844*	*2.19316*
Ni1-S2	2.1598(7)	2.1741(9)	2.1522(8)	-	2.1646(9)	2.1548(5)
	2.18897	*2.19483*	*2.19293*	*2.18901*	*2.19420*	*2.19361*
S1-C5/10[a]	1.767(3)	1.760(3)	1.750(3)	-	1.765(3)	1.7487(16)
	1.77789	*1.77594*	*1.76142*	*1.77762*	*1.77558*	*1.76131*
S2-C6/11[a]	1.768(3)	1.753(3)	1.746(3)	-	1.749(3)	1.7428(14)
	1.77767	*1.76312*	*1.76150*	*1.77568*	*1.76134*	*1.75920*
N1-C1	1.303(3)	1.303(4)	1.299(4)	-	1.311(4)	1.3018(17)
	1.30308	*1.30308*	*1.29798*	*1.30364*	*1.30393*	*1.29850*
N1-N2	1.378(3)	1.376(4)	1.395(3)	-	1.383(4)	1.3906(18)
	1.35229	*1.34658*	*1.35853*	*1.35083*	*1.34529*	*1.35761*

N2-C5/10[a]	1.315(3)	1.319(4)	1.308(4)	-	1.333(4)	1.3060(19)
	1.31508	*1.31937*	*1.30335*	*1.31646*	*1.32063*	*1.30417*
N3-C2	1.305(2)	1.304(4)	1.307(4)	-	1.312(4)	1.3036(18)
	1.30297	*1.29975*	*1.29792*	*1.30802*	*1.30420*	*1.30253*
N3-N4	1.375(3)	1.386(3)	1.389(3)	-	1.378(4)	1.3714(19)
	1.35185	*1.36181*	*1.35845*	*1.34695*	*1.35817*	*1.35409*
N4-C6/C11[a]	1.319(3)	1.303(4)	1.313(4)	-	1.302(4)	1.3122(18)
	1.31546	*1.30021*	*1.30334*	*1.31799*	*1.30238*	*1.30594*
C1-C2	1.470(3), *1.46383*	1.473(4)	1.489(4)	-	1.478(5)	1.487(2)
		1.46728	*1.47456*	*1.46492*	*1.46871*	*1.47614*
Bond Angles (°)						
N3-Ni1-N1	83.59(9)	83.38(11)	83.25(10)	-	83.53(11)	83.30(6)
	83.812	*83.572*	*83.404*	*83.838*	*83.593*	*83.425*
N3-Ni1-S1	170.61(7)	170.54(8)	171.29(8)	-	170.84(8)	171.08(4)
	170.981	*170.759*	*170.579*	*170.935*	*170.795*	*170.607*
N1-Ni1-S1	87.07(6)	87.18(8)	88.06(7)	-	87.49(8)	87.83(4)
	87.169	*87.187*	*87.177*	*87.097*	*87.202*	*87.182*
N3-Ni1-S2	87.56(7)	87.27(8)	87.65(8)	-	87.67(8)	88.17(4)
	87.123	*87.113*	*87.193*	*87.300*	*87.256*	*87.325*
N1-Ni1-S2	171.04(6)	170.50(8)	170.89(8)	-	170.86(8)	171.46(4)
	170.935	*170.686*	*170.595*	*171.137*	*170.846*	*170.751*
S1-Ni1-S2	101.81(3)	102.15(3)	101.04(3)	-	101.37(3)	100.706(16)
	101.895	*102.127*	*102.227*	*101.765*	*101.949*	*102.067*

[a]C5 and C6 for **1** – **3** and C10 and C11 for **4** – **6**.

Electrochemical Characterization

The cyclic voltammograms of all six complexes show two reversible reduction events in acetonitrile (Figure 5a). The observed potentials for **1**,[15] **2**,[12] **4**, and **5**[12] are consistent with prior reports. Previous studies of **1** and related complexes assigned the first reduction as ligand-centered and the second reduction as metal-centered.[15,52,54] These assignments are confirmed by computational studies of **1** described herein, whereas our calculations of **2** – **6** suggest the second reduction is also ligand centered. Ligand modification leads to large changes in potential of both events (Figure 5b, Table 2). For **1** – **3**, the first reduction potential (E_1) shifts anodically by ~180 mV and the second reduction potential (E_2) by ~100 mV for each substitution of a thiosemicarbazonato NHMe with a ethylthiocarbamate OEt (Ni(BTSC) → Ni(TSTC) → Ni(BATC). The same trends are observed for **4** – **6**. The results are consistent with the better donor ability of the thiosemicarbazonato group relative to the ethylthiocarbamate. Further, when one of the backbone methyl groups is replaced by a phenyl group, the reduction potential for both events decrease by ~140 mV. As shown in Figure 5b, the trends are consistent across the series and the effects are predictable and additive. Overall, the first reduction potential can be modulated over a 490 mV window from -1.73 V for **1** to -1.24 V for **6** with the range for the second potential spanning 360 mV.

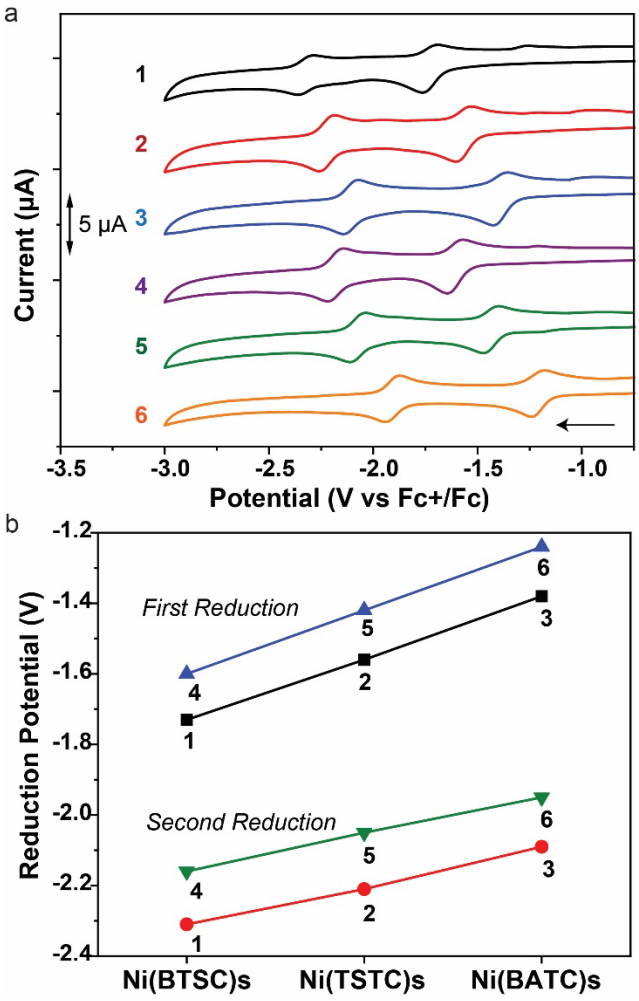

Figure 5. (a) Cyclic voltammograms of **1** – **6** (0.3 mM in MeCN containing 0.1 M NBu_4PF_6 (b) Graphical representation of change in first and second reduction potentials of compounds **1** – **6**.

Table 2. Electrochemical potentials and HER parameters for **1** – **6**.

Complex	E_1 (V)	E_2 (V)	$E_{cat/2}$ (V)	η (V)
1	-1.73	-2.31	-1.99	0.76
2	-1.56	-2.21	-2.02	0.79
3	-1.38	-2.09	-2.02	0.79
4	-1.60	-2.16	-2.03	0.80
5	-1.42	-2.05	-2.05	0.82
6	-1.24	-1.95	-2.05	0.82

Computational Studies

To explore the effect of ligand variation on reduction potential and ligand basicity for **1** – **6**, a series of density functional theory (DFT) calculations were performed on various protonation and charge states. Benchmarking of the functional and basis set was done using complex **2** with B3PW91/TZVP with a PCM solvation model (acetonitrile) giving the best agreement with the experimental results (Tables S3 – S7 and Figure S11). All further calculations were performed using this level of theory. The thermodynamic feasibility of protonation and reduction events was evaluated by calculating acid dissociation equilibrium constants (pK_a) and reduction potentials (E_1 and E_2), respectively. A summary of the calculations can be found in the Supporting Information.

Each of the complexes **1** – **6** were optimized in three different charge states: NiL (S = 0 or 1, q = 0), $[NiL]^{-}$ (S = 1/2, q = −1), and $[NiL]^{2-}$ (S = 0 or 1 q = −2), where S refers to the overall spin and q represents the complex charge. For NiL and $[NiL]^{2-}$, the singlet spin states were lower than the triplet spin states for all complexes by at least 2.36 kcal/mol (Table S8). The calculated reduction potentials for the $[NiL]^{0/-}$ (E_1) and $[NiL]^{-/2-}$ (E_2) were consistent with the experimental values, Figure 6. For all complexes, over 91% of the spin density of the mono reduced derivative $[NiL]^{-}$ lies on the ligand indicating that the first reductions are ligand-centered. Since the two electron reduced species $[NiL]^{2-}$ are closed shell singlets, the electronic structure could be described as Ni(II) with a fully reduced $(L)^{4-}$ ligand or Ni(0) with a dianionic ligand $(L)^{2-}$. The former assignment is preferred as the dx^2-y^2 orbital (LUMO, Figures S12) for each complex remains vacant and bond distances in the ligand backbone are consistent C-N and C=C bonds indicating reduction of the ligand to a tetra-anion (Table S9).

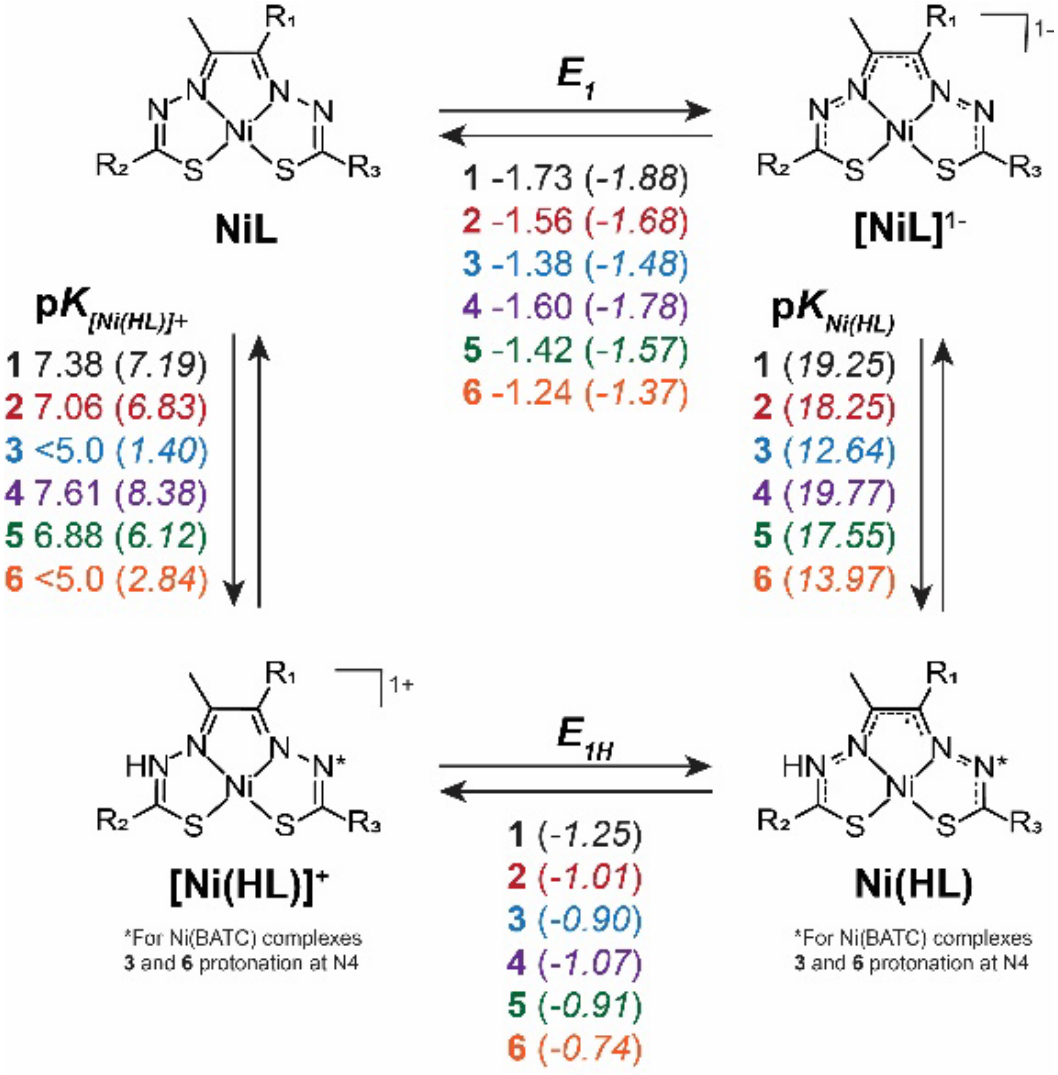

Figure 6. Experimental and computational (*in parentheses*) thermodynamic values for the reduction potential (V) and protonation of **1** – **6**. See Figure 2 for identities of R_1, R_2, and R_3 in **1** – **6**.

Next, the protonation of the neutral complexes **1** – **6** was explored by considering protonation at the heteroatoms (Figures S13 – S18). For complexes **1** – **3** protonation of the non-coordinating hydrazino nitrogen N2 is favored by at least 5 kcal/mol over all other sites. For complexes **4** – **6**, the presence of the phenyl substituent in the ligand backbone results in two

distinct non-coordinating hydrazino nitrogens (N2 and N4), which have similar basicities with optimized energies within ~2 kcal/mol for each site (Figure S15). For complexes **1**, **2**, **4**, and **5** the calculated pK_a values are ~0.2 pK_a units lower than experimental values. For **3** and **6**, for which experimental pK_a values could not be measured, the computational values of 1.40 and 2.84 are consistent with their low basicity, Figure 6. Protonation shifts the first and second reduction potential for each complex by ~600 mV. Notably, this results in the second reduction potential of the protonated derivatives to be more accessible than the first reduction of the neutral species. For the monoprotonated species **1-H** the metal centered spin-density is slightly increased to 13.71% compared with 8.49% metal centered spin density in $\mathbf{1}^-$ (Table S10 and S11 and Figures S19– S20). This indicates that partial charge neutralization of the ligand via protonation shifts unpaired electron spin towards the metal center. The same trend is observed for the other complexes.

The addition of a second electron to the monoprotonated species Ni(HL) can yield a singlet or triplet spin state which may facilitate proton transfer from a non-coordinating hydrazino N to a different basic site. As such, we considered protonation at the Ni and all heteroatoms. In complex $\mathbf{[1\text{-}H]}^-$, a triplet ground state metal hydride is slightly favored in energy relative to the singlet state with ligand hydride in which the proton is observed on one of the coordinated nitrogen donors. Thus, reduction of **1-H** favors proton tautomerization from an uncoordinated nitrogen to the metal center to generate a metal hydride. In contrast, for complexes **2-H** and **3-H**, the singlet state ligand hydride tautomers are lower in energy than the triplet metal hydrides by 4.4 and 5.9 kcal/mol, respectively. For complexes **4-H** to **6-H**, substitution of a methyl backbone substituent with a phenyl further increases the singlet-triplet gap (Table S12). Overall, there is a divergence at the point of hydride formation with complex **1** favoring a metal hydride and **2** – **6** favoring ligand hydrides.

Hydrogen Evolution Reaction

Complexes **1** – **6** were investigated for their activity as homogeneous electrocatalysts for the hydrogen evolution reaction (HER) in acetonitrile. Results are compiled in Table 2. Titration of a 0.3 mM solution of each complex in acetonitrile under argon with increasing quantities of acetic acid led to large current increases in the cathodic region indicative of electrocatalytic proton reduction (Figure S21). Representative CVs for each of the catalysts in the presence of 350 mM acetic acid are given in Figure 7. In the presence of acid, the two reversible reduction events of the complexes were replaced by a small irreversible precatalytic event and one irreversible catalytic event. The precatalytic event is attributed to a precatalyst transformation to a heterogenous adsorbed catalyst. [55-59]

As seen in Table 2, the value of $E_{cat/2}$ and overpotential (η) for the six different complexes vary by only 60 mV, despite the clear differences observed for their reduction potentials in the absence of acid. This observation strongly suggests the complexes are degrading to a common catalytically active species under HER conditions. In support of this hypothesis, HER activity in presence of 350 mM acetic acid did not exhibit linear dependance on the catalyst concentration (Figure S22). To further confirm this, long-term activity test using chronoamperometry at a constant potential of $E_{cat/2}$ for 2 hours in the presence of 350 mM acetic acid were conducted for **1** and **6**. Dip tests of the electrodes, after chronoamperometric measurements, in fresh solutions containing 350 mM acetic acid revealed catalytic currents similar to those observed for solutions of **1** – **6** (Figure S23) indicating formation of a catalytically active film during HER.

In an attempt to further confirm the formation of a heterogenous catalyst on the electrode surface, a mercury test was performed by soaking an electrode containing material deposited during a CA experiment in mercury, although this method has known limitations.[60-62] As shown

in Figure S25, CA for 2 hours in the presence of **1** and 350 mM acetic acid yields a catalytically active film that yields significant current when placed in a blank solution containing 350 mM acetic acid. However, after soaking in a pool of Hg for 3 hours, the catalytic current is diminished by ~50% with a further current decrease observed after 6 hours. The results are consistent the formation of an amalgam between the heterogeneous catalyst and Hg. However, control experiments (Figure S23) show reactivity between solutions of **1** and Hg and interaction between Hg and intact **1** absorbed on the electrode cannot be excluded as a possible explanation.

The observed degradation of **1** – **6** under electrocatalytic HER conditions in MeCN is contrast to prior studies reported in DMF. For example, dip tests reported by Jain et al. showed no evidence of complex degradation after electrocatalytic experiments with 1 in DMF.[15] Similarly, a series of NiN_2S_2 complexes were reported by Papadakis as homogeneous HER catalytsts in DMF.[20] Interestingly, in the current study dip tests of electrodes after chronoamperometric reduction of **1** and **6** in the *absence of acid* showed no signs of film formation (Figure S23) indicating that both acid and reducing conditions are required for film formation. Attempts to prevent film formation by varying the concentration of acid were unsuccessful. In all cases **1** – **6** displayed overpotentials similar to each other and to the simple nickel salt $Ni(OTf)_2$ (Figure S27 and Table S13). Thus, the experimental conditions including various factors such as solvent, reduction potential, and acid need to be considered when evaluating catalyst stability.

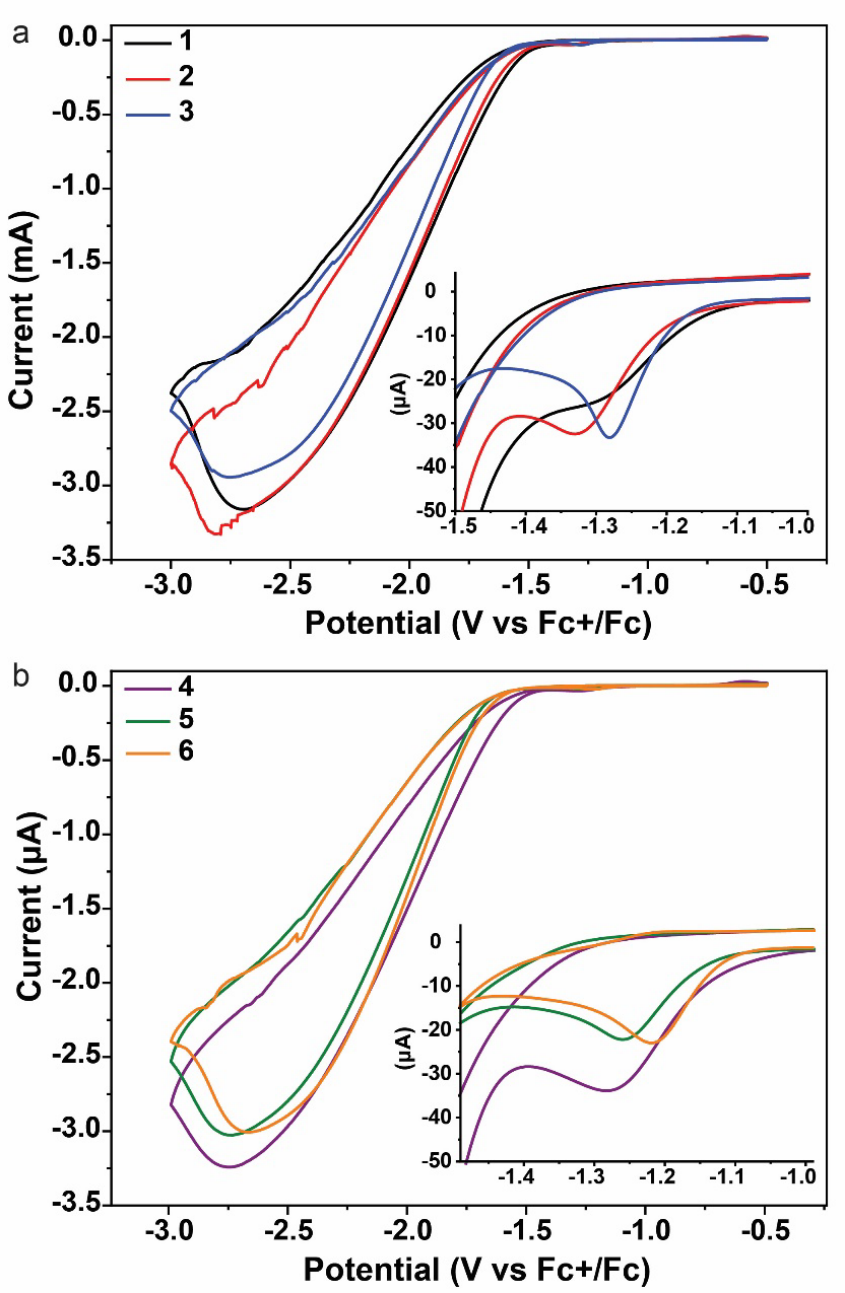

Figure 7. Cyclic voltammogram of (a) **1** – **3** and (b) **4** – **6** with 350 mM acetic acid showing an irreversible catalytic event (0.3 mM in MeCN containing 0.1 M NBu_4PF_6, υ = 200 mV/s, glassy carbon working electrode, Ag wire quasi-reference electrode, and a Pt wire counter electrode). The insets show expanded views of the precatalytic events.

Conclusions

A series of BTSC, TSTC and BTAC ligands have been designed to modulate the electronic structure of Ni(II) complexes containing an N_2S_2 core by variation of the pendent and backbone functional groups. This resulted in systematic shifts in reduction potentials to more anodic potentials for each substitution of a thiosemicarbazonato NHMe with an ethylthiocarbamato OEt group (Ni(BTSC) $\rightarrow$ Ni(TSTC) $\rightarrow$ Ni(BATC). We also quantified the changes in the ligand basicity associated with changes in ligand framework structure both experimentally as well as computationally with basicity decreasing accordingly, BTSC > TSTC > BTAC. Within the series of complexes the reduction potentials vary over an ~500 mV range and the ligand basicity over ~7 pK_a units. DFT calculations predicted a divergence of HER mechanism of catalysts and improvement of electrocatalytic HER activity of BATC and TSTC nickel complexes. For all complexes, the calculated pK_a values of neutral complexes are ≤ 8.38 making protonation even by stronger acids prior to reduction unfavorable. Experimental evidence shows that all the catalysts are stable under reducing or acidic conditions, however, the combination of both leads to ligand degradation forming a common nickel species and deposition of an electroactive film on the glassy carbon electrode surface under the experimental conditions. Evaluation of these complexes as heterogeneous water splitting electrocatalysts in aqueous solutions are in progress and will be the subject of a future publication.

References

1. Gennari, M.; Duboc, C., Bio-inspired, Multifunctional Metal–Thiolate Motif: From Electron Transfer to Sulfur Reactivity and Small-Molecule Activation. *Accounts of Chemical Research* **2020,** *53* (11), 2753-2761. DOI: 10.1021/acs.accounts.0c00555

2. Forbes, C. E.; Gold, A.; Holm, R. H., Complete electron-transfer series of the Pt-N2S2 type. *Inorganic Chemistry* **1971,** *10* (11), 2479-2485. DOI: 10.1021/ic50105a022

3. McCleverty, J. A., Metal 1,2-Dithiolene and Related Complexes. In *Progress in Inorganic Chemistry*, 1968; pp 49-221.

4. West, D. X.; Ives, J. S.; Bain, G. A.; Liberta, A. E.; Valdés-Martínez, J.; Ebert, K. H.; Hernández-Ortega, S., Copper(II) and nickel(II) complexes of 2,3-butanedione bis(N(3)-substituted thiosemicarbazones). *Polyhedron* **1997,** *16* (11), 1895-1905. DOI: 10.1016/S0277-5387(96)00468-8

5. Mckenzie-Nickson, S.; Bush, A.; J Barnham, K., Bis (thiosemicarbazone) metal complexes as therapeutics for neurodegenerative diseases. *Current Topics in Medicinal Chemistry* **2016,** *16* (27), 3058-3068. DOI:

6. Fujibayashi, Y.; Taniuchi, H.; Yonekura, Y.; Ohtani, H., Copper-62-ATSM: a new hypoxia imaging agent with high membrane permeability and low redox potential. *The Journal of Nuclear Medicine* **1997,** *38* (7), 1155. DOI:

7. Palanimuthu, D.; Shinde, S. V.; Somasundaram, K.; Samuelson, A. G., In Vitro and in Vivo Anticancer Activity of Copper Bis(thiosemicarbazone) Complexes. *Journal of Medicinal Chemistry* **2013,** *56* (3), 722-734. DOI: 10.1021/jm300938r

8. Genova, P.; Varadinova, T.; Matesanz, A. I.; Marinova, D.; Souza, P., Toxic effects of bis(thiosemicarbazone) compounds and its palladium(II) complexes on herpes simplex virus growth. *Toxicology and Applied Pharmacology* **2004,** *197* (2), 107-112. DOI: 10.1016/j.taap.2004.02.006

9. Lessa, J. A.; Reis, D. C.; Da Silva, J. G.; Paradizzi, L. T.; da Silva, N. F.; de Fátima A. Carvalho, M.; Siqueira, S. A.; Beraldo, H., Coordination of Thiosemicarbazones and Bis(thiosemicarbazones) to Bismuth(III) as a Strategy for the Design of Metal-Based

Antibacterial Agents. *Chemistry & Biodiversity* **2012,** *9* (9), 1955-1966. DOI: 10.1002/cbdv.201100447

10. Bajaj, K.; Buchanan, R. M.; Grapperhaus, C. A., Antifungal activity of thiosemicarbazones, bis(thiosemicarbazones), and their metal complexes. *J. Inorg. Biochem.* **2021,** *225*. DOI: 10.1016/j.jinorgbio.2021.111620

11. Vishnosky, N. S.; Mashuta, M. S.; Buchanan, R. M.; Grapperhaus, C. A., Syntheses, structures, and electrochemical studies of N, N′-bis (alkylthiocarbamate) butane-2, 3-diimine Cu (II) complexes as pendent alkoxy derivatives of Cu (ATSM). *Inorganica Chimica Acta* **2017,** *461*, 45-51. DOI: 10.1016/j.ica.2017.02.003

12. Andres, S. A.; Bajaj, K.; Vishnosky, N. S.; Peterson, M. A.; Mashuta, M. S.; Buchanan, R. M.; Bates, P. J.; Grapperhaus, C. A., Synthesis, Characterization, and Biological Activity of Hybrid Thiosemicarbazone–Alkylthiocarbamate Metal Complexes. *Inorganic Chemistry* **2020,** *59* (7), 4924-4935. DOI: 10.1021/acs.inorgchem.0c00182

13. Haddad, A. Z.; Garabato, B. D.; Kozlowski, P. M.; Buchanan, R. M.; Grapperhaus, C. A., Beyond Metal-Hydrides: Non-Transition-Metal and Metal-Free Ligand-Centered Electrocatalytic Hydrogen Evolution and Hydrogen Oxidation. *J Am Chem Soc* **2016,** *138* (25), 7844-7847. DOI: 10.1021/jacs.6b04441

14. Haddad, A. Z.; Cronin, S. P.; Mashuta, M. S.; Buchanan, R. M.; Grapperhaus, C. A., Metal-Assisted Ligand-Centered Electrocatalytic Hydrogen Evolution upon Reduction of a Bis(thiosemicarbazonato)Cu(II) Complex. *Inorganic Chemistry* **2017,** *56* (18), 11254-11265. DOI: 10.1021/acs.inorgchem.7b01608

15. Jain, R.; Mamun, A. A.; Buchanan, R. M.; Kozlowski, P. M.; Grapperhaus, C. A., Ligand-Assisted Metal-Centered Electrocatalytic Hydrogen Evolution upon Reduction of a

Bis(thiosemicarbazonato)Ni(II) Complex. *Inorganic Chemistry* **2018,** *57* (21), 13486-13493. DOI: 10.1021/acs.inorgchem.8b02110

16. Gupta, A. J.; Vishnosky, N. S.; Hietsoi, O.; Losovyj, Y.; Strain, J.; Spurgeon, J.; Mashuta, M. S.; Jain, R.; Buchanan, R. M.; Gupta, G.; Grapperhaus, C. A., Effect of Stacking Interactions on the Translation of Structurally Related Bis(thiosemicarbazonato)nickel(II) HER Catalysts to Modified Electrode Surfaces. *Inorganic Chemistry* **2019,** *58* (18), 12025-12039. DOI: 10.1021/acs.inorgchem.9b01209

17. Gulati, S.; Hietsoi, O.; Calvary, C. A.; Strain, J. M.; Pishgar, S.; Brun, H. C.; Grapperhaus, C. A.; Buchanan, R. M.; Spurgeon, J. M., Photocatalytic hydrogen evolution on Si photocathodes modified with bis(thiosemicarbazonato)nickel(ii)/Nafion. *Chemical Communications* **2019,** *55* (64), 9440-9443. DOI: 10.1039/C9CC04117F

18. Paudel, M.; Daniels, B.; Arts, A. M.; Gupta, A.; Kalbfleisch, T.; Hofsommer, D. T.; Grapperhaus, C. A.; Buchanan, R. M.; Gupta, G., Unravelling the potential of disposable and modifiable pencils as catalyst supports for hydrogen evolution reaction. *New Journal of Chemistry* **2022,** *46* (39), 18832-18838. DOI: 10.1039/D2NJ03359C

19. Barrozo, A.; Orio, M., Unraveling the catalytic mechanisms of H2 production with thiosemicarbazone nickel complexes. *RSC Advances* **2021,** *11* (9), 5232-5238. DOI: 10.1039/D0RA10212A

20. Papadakis, M.; Barrozo, A.; Straistari, T.; Queyriaux, N.; Putri, A.; Fize, J.; Giorgi, M.; Réglier, M.; Massin, J.; Hardré, R.; Orio, M., Ligand-based electronic effects on the electrocatalytic hydrogen production by thiosemicarbazone nickel complexes. *Dalton Transactions* **2020,** *49* (16), 5064-5073. DOI: 10.1039/C9DT04775A

21. Drosou, M.; Kamatsos, F.; Mitsopoulou, C. A., Recent advances in the mechanisms of the hydrogen evolution reaction by non-innocent sulfur-coordinating metal complexes. *Inorg. Chem. Front.* **2020,** *7* (1), 37-71. DOI: 10.1039/C9QI01113G

22. Luo, G.-G.; Zhang, H.-L.; Tao, Y.-W.; Wu, Q.-Y.; Tian, D.; Zhang, Q., Recent progress in ligand-centered homogeneous electrocatalysts for hydrogen evolution reaction. *Inorg. Chem. Front.* **2019,** *6* (2), 343-354. DOI: 10.1039/C8QI01220B

23. Phipps, C. A.; Hofsommer, D. T.; Toda, M. J.; Nkurunziza, F.; Shah, B.; Spurgeon, J. M.; Kozlowski, P. M.; Buchanan, R. M.; Grapperhaus, C. A., Ligand-Centered Hydrogen Evolution with Ni(II) and Pd(II)DMTH. *Inorganic Chemistry* **2022,** *61* (25), 9792-9800. DOI: 10.1021/acs.inorgchem.2c01326

24. Reüfenacht, K., Arbetien über Phosphosäure- und Thiosphosphorsäureester mit einem Heterocyclischen Substituenten Thiadiazol-Ringschluss und eine Dabei Auftretende Methylübertragung. *Helv Chim Acta* **1972,** *55*, 1178-1187. DOI: 10.1002/hlca.19720550414

25. Beraldo, H.; Kaisner, S. B.; Turner, J. D.; Billeh, I. S.; Ives, J. S.; West, D., Copper (II) and nickel (II) complexes of the bis {N (3)-substituted thiosemicarbazones} of phenylglyoxal and 1-phenylpropane-1, 2-dione. *Transition Metal Chemistry* **1997,** *22*, 459-464. DOI: 10.1023/A:1018503011264

26. Tshepelevitsh, S.; Kütt, A.; Lõkov, M.; Kaljurand, I.; Saame, J.; Heering, A.; Plieger, P. G.; Vianello, R.; Leito, I., On the Basicity of Organic Bases in Different Media. *European Journal of Organic Chemistry* **2019,** *2019* (40), 6735-6748. DOI: 10.1002/ejoc.201900956

27. Fourmond, V.; Jacques, P.-A.; Fontecave, M.; Artero, V., H2 Evolution and Molecular Electrocatalysts: Determination of Overpotentials and Effect of Homoconjugation. *Inorganic Chemistry* **2010,** *49* (22), 10338-10347. DOI: 10.1021/ic101187v

28. Kütt, A.; Tshepelevitsh, S.; Saame, J.; Lõkov, M.; Kaljurand, I.; Selberg, S.; Leito, I., Strengths of Acids in Acetonitrile. *European Journal of Organic Chemistry* **2021,** *2021* (9), 1407-1419. DOI: 10.1002/ejoc.202001649

29. Appel, A. M.; DuBois, D. L.; Rakowski DuBois, M., Molybdenum−Sulfur Dimers as Electrocatalysts for the Production of Hydrogen at Low Overpotentials. *J Am Chem Soc* **2005,** *127* (36), 12717-12726. DOI: 10.1021/ja054034o

30. Costentin, C.; Drouet, S.; Robert, M.; Savéant, J.-M., Turnover Numbers, Turnover Frequencies, and Overpotential in Molecular Catalysis of Electrochemical Reactions. Cyclic Voltammetry and Preparative-Scale Electrolysis. *J Am Chem Soc* **2012,** *134* (27), 11235-11242. DOI: 10.1021/ja303560c

31. Burke, K., Perspective on density functional theory. *J. Chem. Phys.* **2012,** *136* (15), 150901. DOI: 10.1063/1.4704546

32. Kohn, W.; Becke, A. D.; Parr, R. G., Density Functional Theory of Electronic Structure. *J. Phys. Chem.* **1996,** *100* (31), 12974-12980. DOI: 10.1021/jp960669l

33. Vosko, S. H.; Wilk, L.; Nusair, M., Accurate spin-dependent electron liquid correlation energies for local spin density calculations: a critical analysis. *Canadian Journal of physics* **1980,** *58* (8), 1200-1211. DOI: 10.1139/p80-159

34. Lee, C.; Yang, W.; Parr, R. G., Development of the Colle-Salvetti correlation-energy formula into a functional of the electron density. *Physical Review B* **1988,** *37* (2), 785-789. DOI: 10.1103/PhysRevB.37.785

35. Becke, A. D., A new mixing of Hartree–Fock and local density-functional theories. *Journal of chemical physics* **1993,** *98* (2), 1372-1377. DOI: 10.1063/1.464304

36. Perdew, J. P., Density-functional approximation for the correlation energy of the inhomogeneous electron gas. *Physical Review B* **1986,** *33* (12), 8822-8824. DOI: 10.1103/PhysRevB.33.8822

37. Perdew, J. P.; Ziesche, P.; Eschrig, H., Electronic structure of solids' 91.

38. Grimme, S., Semiempirical GGA-type density functional constructed with a long-range dispersion correction. *Journal of Computational Chemistry* **2006,** *27* (15), 1787-1799. DOI: 10.1002/jcc.20495

39. Zhao, Y.; Truhlar, D. G., A new local density functional for main-group thermochemistry, transition metal bonding, thermochemical kinetics, and noncovalent interactions. *Journal of Chemical Physics* **2006,** *125* (19). DOI: 10.1063/1.2370993

40. Chai, J.-D.; Head-Gordon, M., Long-range corrected hybrid density functionals with damped atom–atom dispersion corrections. *Physical Chemistry Chemical Physics* **2008,** *10* (44), 6615-6620. DOI: 10.1039/B810189B

41. Krishnan, R.; Binkley, J. S.; Seeger, R.; Pople, J. A., Self-consistent molecular orbital methods. XX. A basis set for correlated wave functions. *Journal of Chemical Physics* **2008,** *72* (1), 650-654. DOI: 10.1063/1.438955

42. McLean, A. D.; Chandler, G. S., Contracted Gaussian basis sets for molecular calculations. I. Second row atoms, Z=11–18. *Journal of Chemical Physics* **2008,** *72* (10), 5639-5648. DOI: 10.1063/1.438980

43. Schäfer, A.; Horn, H.; Ahlrichs, R., Fully optimized contracted Gaussian basis sets for atoms Li to Kr. *Journal of Chemical Physics* **1992,** *97* (4), 2571-2577. DOI: 10.1063/1.463096

44. Tomasi, J.; Mennucci, B.; Cammi, R., Quantum Mechanical Continuum Solvation Models. *Chemical Reviews* **2005,** *105* (8), 2999-3094. DOI: 10.1021/cr9904009

45. Frisch, M. J.; Trucks, G. W.; Schlegel, H. B.; Scuseria, G. E.; Robb, M. A.; Cheeseman, J. R.; Scalmani, G.; Barone, V.; Petersson, G. A.; Nakatsuji, H.; Li, X.; Caricato, M.; Marenich, A. V.; Bloino, J.; Janesko, B. G.; Gomperts, R.; Mennucci, B.; Hratchian, H. P.; Ortiz, J. V.; Izmaylov, A. F.; Sonnenberg, J. L.; Williams; Ding, F.; Lipparini, F.; Egidi, F.; Goings, J.; Peng, B.; Petrone, A.; Henderson, T.; Ranasinghe, D.; Zakrzewski, V. G.; Gao, J.; Rega, N.; Zheng, G.; Liang, W.; Hada, M.; Ehara, M.; Toyota, K.; Fukuda, R.; Hasegawa, J.; Ishida, M.; Nakajima, T.; Honda, Y.; Kitao, O.; Nakai, H.; Vreven, T.; Throssell, K.; Montgomery Jr., J. A.; Peralta, J. E.; Ogliaro, F.; Bearpark, M. J.; Heyd, J. J.; Brothers, E. N.; Kudin, K. N.; Staroverov, V. N.; Keith, T. A.; Kobayashi, R.; Normand, J.; Raghavachari, K.; Rendell, A. P.; Burant, J. C.; Iyengar, S. S.; Tomasi, J.; Cossi, M.; Millam, J. M.; Klene, M.; Adamo, C.; Cammi, R.; Ochterski, J. W.; Martin, R. L.; Morokuma, K.; Farkas, O.; Foresman, J. B.; Fox, D. J. *Gaussian 16 Rev. C.01*, Wallingford, CT, 2016.

46. Andrienko, G. A. *ChemCraft - graphical software for visualization of quantum chemistry computations, version 1.8 (build 654)*, www.chemcraftprog.com.

47. Dennington, R. K., Todd A.; Millam, John M. *GaussView, Version 6*, Semichem Inc., Shawnee Mission , KS, 2016.

48. Roy, L. E.; Jakubikova, E.; Guthrie, M. G.; Batista, E. R., Calculation of One-Electron Redox Potentials Revisited. Is It Possible to Calculate Accurate Potentials with Density Functional Methods? *J. Phys. Chem. A* **2009,** *113* (24), 6745-6750. DOI: 10.1021/jp811388w

49. *CrysalisPro Software System (CCD and RED), V 1.171.40.67a*, Rigaku Oxford Diffraction, Oxford, UK, 2019.

50. *SCALE3 ABSPACK included in CrysAlis PRO RED, V 1.171.40.67a*, Rigaku Oxford Diffraction, Oxford, UK, 2019.

51. Sheldrick, G., M., A short history of SHELX. *Acta Crystallogr. A* **2008,** *64* (1), 112-122. DOI: doi:10.1107/S0108767307043930

52. Calvary, C. A.; Hietsoi, O.; Strain, J. M.; Mashuta, M. S.; Spurgeon, J. M.; Buchanan, R. M.; Grapperhaus, C. A., Synthesis, Characterization, and HER Activity of Pendant Diamine Derivatives of NiATSM. *Eur J Inorg Chem* **2019,** *2019* (33), 3782-3790. DOI: 10.1002/ejic.201900721

53. Blower, P. J.; Castle, T. C.; Cowley, A. R.; Dilworth, J. R.; Donnelly, P. S.; Labisbal, E.; Sowrey, F. E.; Teat, S. J.; Went, M. J., Structural trends in copper(ii) bis(thiosemicarbazone) radiopharmaceuticals. *Dalton Transactions* **2003,** (23), 4416-4425. DOI: 10.1039/B307499D

54. Straistari, T.; Fize, J.; Shova, S.; Réglier, M.; Artero, V.; Orio, M., A Thiosemicarbazone–Nickel(II) Complex as Efficient Electrocatalyst for Hydrogen Evolution. *ChemCatChem* **2017,** *9* (12), 2262-2268. DOI: 10.1002/cctc.201600967

55. Lee, K. J.; McCarthy, B. D.; Dempsey, J. L., On decomposition, degradation, and voltammetric deviation: the electrochemist's field guide to identifying precatalyst transformation. *Chemical Society Reviews* **2019,** *48* (11), 2927-2945. DOI: 10.1039/C8CS00851E

56. Anxolabéhère-Mallart, E.; Costentin, C.; Fournier, M.; Nowak, S.; Robert, M.; Savéant, J.-M., Boron-Capped Tris(glyoximato) Cobalt Clathrochelate as a Precursor for the Electrodeposition of Nanoparticles Catalyzing H2 Evolution in Water. *J Am Chem Soc* **2012,** *134* (14), 6104-6107. DOI: 10.1021/ja301134e

57. Kaeffer, N.; Morozan, A.; Fize, J.; Martinez, E.; Guetaz, L.; Artero, V., The Dark Side of Molecular Catalysis: Diimine–Dioxime Cobalt Complexes Are Not the Actual Hydrogen

Evolution Electrocatalyst in Acidic Aqueous Solutions. *ACS Catalysis* **2016,** *6* (6), 3727-3737. DOI: 10.1021/acscatal.6b00378

58. Martin, D. J.; McCarthy, B. D.; Donley, C. L.; Dempsey, J. L., Electrochemical hydrogenation of a homogeneous nickel complex to form a surface adsorbed hydrogen-evolving species. *Chemical Communications* **2015,** *51* (25), 5290-5293. DOI: 10.1039/C4CC08662G

59. McCarthy, B. D.; Donley, C. L.; Dempsey, J. L., Electrode initiated proton-coupled electron transfer to promote degradation of a nickel(ii) coordination complex. *Chemical Science* **2015,** *6* (5), 2827-2834. DOI: 10.1039/C5SC00476D

60. Kaeffer, N.; Morozan, A.; Fize, J.; Martinez, E.; Guetaz, L.; Artero, V., The Dark Side of Molecular Catalysis: Diimine-Dioxime Cobalt Complexes Are Not the Actual Hydrogen Evolution Electrocatalyst in Acidic Aqueous Solutions. *ACS Catal.* **2016,** *6* (6), 3727-3737. DOI: 10.1021/acscatal.6b00378

61. Artero, V.; Fontecave, M., Solar fuels generation and molecular systems: is it homogeneous or heterogeneous catalysis? *Chemical Society Reviews* **2013,** *42* (6), 2338-2356. DOI: 10.1039/C2CS35334B

62. Chernyshev, V. M.; Astakhov, A. V.; Chikunov, I. E.; Tyurin, R. V.; Eremin, D. B.; Ranny, G. S.; Khrustalev, V. N.; Ananikov, V. P., Pd and Pt Catalyst Poisoning in the Study of Reaction Mechanisms: What Does the Mercury Test Mean for Catalysis? *ACS Catalysis* **2019,** *9* (4), 2984-2995. DOI: 10.1021/acscatal.8b03683

Supporting Information.

The following files are available free of charge. Sample calculations and NMR, IR, UV-vis, cyclic voltammograms, chronopotentiometry, computational, and x-ray data are included (PDF). CCDC 2288054 and 2288055 contain the supplementary crystallographic data for this paper. These data

can be obtained free of charge via www.ccdc.cam.ac.uk/data_request/cif, or by emailing data_request@ccdc.cam.ac.uk, or by contacting The Cambridge Crystallographic Data Centre, 12 Union Road, Cambridge CB2 1EZ, UK; fax: +44 1223 336033.

Corresponding Author

Craig Grapperhaus email: craig.grapperhaus@louisville.edu

Robert Buchanan email: robert.buchanan@louisville.edu

Author Contributions

S.K. performed pK_a experiments and DFT computations and interpretations and contributed to the writing of manuscript. S. P. and P.M.K. supervised the DFT computations. K.B. synthesized some of the ligands and metal complexes. M.S.M. performed all crystallographic studies. M.P. performed all other experiments and wrote the initial draft of the manuscript. D.T.H., G.G., R.M.B., and C.A.G. conceived the project, supervised experimental studies, and contributed to writing the manuscript. All authors have approved the final version of the manuscript.

Funding Sources

This research was supported by the National Science Foundation CHE-1955268 (CAG) and CHE-1800245(RMB). The Department of Energy (DEFG02-08CH11538) and the Kentucky Research Challenge Trust Fund are acknowledged for upgrade of the X-ray facility (MSM).

Notes

The authors declare no competing financial interests.

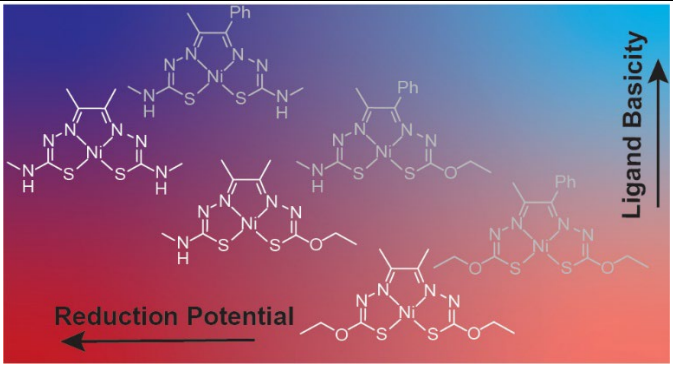

Variation of the pendent groups and backbone substituents modulate the reduction potential over an ~500 mV range and the ligand basicity over ~7 pK_a units.